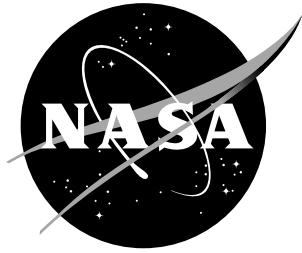# Proper Orthogonal Decomposition in Optimal Control of Fluids

S. S. Ravindran
Langley Research Center, Hampton, Virginia

The NASA STI Program Office ... in Profile

Since its founding, NASA has been dedicated to the advancement of aeronautics and space science. The NASA Scientific and Technical Information (STI) Program Office plays a key part in helping NASA maintain this important role.

The NASA STI Program Office is operated by Langley Research Center, the lead center for NASA's scientific and technical information. The NASA STI Program Office provides access to the NASA STI Database, the largest collection of aeronautical and space science STI in the world. The Program Office is also NASA's institutional mechanism for disseminating the results of its research and development activities. These results are published by NASA in the NASA STI Report Series, which includes the following report types:
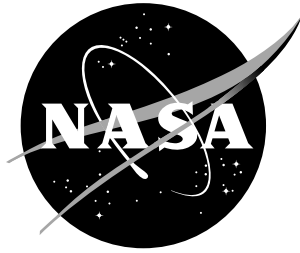
- TECHNICAL PUBLICATION. Reports of completed research or a major significant phase of research that present the results of NASA programs and include extensive data or theoretical analysis. Includes compilations of significant scientific and technical data and information deemed to be of continuing reference value. NASA counterpart of peer-reviewed formal professional papers, but having less stringent limitations on manuscript length and extent of graphic presentations.

- TECHNICAL MEMORANDUM. Scientific and technical findings that are preliminary or of specialized interest, e.g., quick release reports, working papers, and bibliographies that contain minimal annotation. Does not contain extensive analysis.

- CONTRACTOR REPORT. Scientific and technical findings by NASA-sponsored contractors and grantees.

- CONFERENCE PUBLICATION. Collected papers from scientific and technical conferences, symposia, seminars, or other meetings sponsored or co-sponsored by NASA.

- SPECIAL PUBLICATION. Scientific, technical, or historical information from NASA programs, projects, and missions, often concerned with subjects having substantial public interest.

- TECHNICAL TRANSLATION. English-language translations of foreign scientific and technical material pertinent to NASA's mission.

Specialized services that complement the STI Program Office's diverse offerings include creating custom thesauri, building customized databases, organizing and publishing research results ... even providing videos.

For more information about the NASA STI Program Office, see the following:

- Access the NASA STI Program Home Page at *http://www.sti.nasa.gov*

- E-mail your question via the Internet to help@sti.nasa.gov

- Fax your question to the NASA STI Help Desk at (301) 621-0134

- Phone the NASA STI Help Desk at (301) 621-0390

- Write to:
  NASA STI Help Desk
  NASA Center for AeroSpace Information
  7121 Standard Drive
  Hanover, MD 21076-1320

NASA/TM-1999-209113

Proper Orthogonal Decomposition in Optimal Control of Fluids

S. S. Ravindran
Langley Research Center, Hampton, Virginia

March 1999

PROPER ORTHOGONAL DECOMPOSITION IN OPTIMAL CONTROL OF FLUIDS *

S.S. RAVINDRAN[†]

Abstract. In this article, we present a *reduced order modeling* approach suitable for active control of fluid dynamical systems based on proper orthogonal decomposition (POD). The rationale behind the reduced order modeling is that numerical simulation of Navier-Stokes equations is still too costly for the purpose of optimization and control of unsteady flows. We examine the possibility of obtaining reduced order models that reduce computational complexity associated with the Navier-Stokes equations while capturing the essential dynamics by using the POD. The POD allows extraction of certain optimal set of basis functions, perhaps few, from a computational or experimental data-base through an eigenvalue analysis. The solution is then obtained as a linear combination of these optimal set of basis functions by means of Galerkin projection. This makes it attractive for optimal control and estimation of systems governed by partial differential equations. We here use it in active control of fluid flows governed by the Navier-Stokes equations. We show that the resulting reduced order model can be very efficient for the computations of optimization and control problems in unsteady flows. Finally, implementational issues and numerical experiments are presented for simulations and optimal control of fluid flow through channels.

Key words. POD, reduced order model, flow control, optimal control, Galerkin methods.

AMS subject classifications. 93B40, 49M05, 76D05, 49K20, 65M60, 76D15

1. Introduction. The invention of Micro Electro Mechanical Systems and other fast micro-devices has generated substantial interest in active control of fluid dynamical systems for the design of advanced fluid dynamical technology. There are a large number of articles devoted to this actively growing field. For example, in [7, 9, 8, 10, 26, 4] various optimal control problems in viscous incompressible flows were discussed. In [22, 17, 21, 16, 25] experimental efforts were reported. However, efficient computational methodologies for use in on-line, real-time computation for PDE based control design has seen little progress. In this article we discuss a reduced order method for PDE based control using the proper orthogonal decomposition (POD).

The solution of complex fluid dynamic equations using the available finite element, finite volume, finite difference or spectral methods is, in general, not feasible for real-time estimation and control. There are methods that would yield small degree of freedom models for the purpose of control of partial differential equations. However, they do not adequately represent the physics of the system and may be very sensitive to operating conditions as they are based on input/output data of a given system.

We here examine the possibility of obtaining reduced order models that reduces computational complexity associated with the Navier-Stokes equations while capturing the essential dynamics by using the proper orthogonal decomposition (POD). The proper orthogonal decomposition is a model reduction technique for complex nonlinear problems. It was first proposed by Karhunen [11] and Loeve [14] independently and sometimes called Karhunen–Loeve (K–L) expansion. Subsequently it has been applied in various applications. In [15] the method was first called POD and there it was used to study turbulent flows. In [23] another important progress was made and the method of "snapshots" was incorporated into the POD framework which will be

†NRC Research Associate, Flow Modeling and Control Branch, Fluid Mechanics and Acoustics Division, NASA Langley Research Center, Mail Stop 170, Hampton, VA 23681 (s.s.ravindran@larc.nasa.gov, http://fmcb.larc.nasa.gov/~ ravi).

described in the sequel. Other applications in turbulent flow simulations are given in
[1, 24, 2, 18, 3, 20] and [12].

When discretizing nonlinear partial differential equations using finite volume, fi-
nite difference, finite element or spectral methods, one uses basis functions that have
very little connection to the problem or to the underlying partial differential equations.
In some spectral methods Legendre polynomials are used, in finite element methods
piecewise polynomials are used and in finite difference methods grid functions are
used. However, POD uses basis functions that are generated from the numerical
solutions of the system or from the experimental measurements.

The essential idea is to generate optimal basis functions for Galerkin representa-
tions of PDEs. In other words, given an ensemble $\mathcal{S} = \{\mathbf{U}^{(i)}\}_{i=1}^{N}$ consisting of N data
vectors of length N_s, the K–L theory yields that we can find an orthonormal coordi-
nate system $\{\mathbf{V}^{(i)}\}_{i=1}^{N_s}$ that is optimal in the sense that the variance of the dataset in
the coordinate directions becomes maximal. Thus, when the Navier-Stokes equations
are projected onto this optimal base using a Galerkin projection, one obtains a re-
duced order model. The beauty of the POD is that it is a nonlinear model reduction
approach and its mathematical theory is based on the spectral theory of compact, self
adjoint operators.

Our goal here is to discuss a computational approach based on reduced order
models resulting from the application of POD for the active control problems arising
in nonlinear fluid dynamic systems.

As a test problem we take a two-dimensional flow through backward facing step
channel. This flow configuration is considered as a typical unsteady separated flow.
For high Reynolds' numbers, flow separates and recirculation appears. We will for-
mulate a recirculation control problem in this configuration with the control action
achieved through the surface movement/blowing of mass on a part of the boundary.

The plan of the paper is as follows. In the remainder of this section we establish
the notation that will be used throughout the paper. In §2, we present the proper
orthogonal decomposition and its properties. In §3, we describe the prototypical prob-
lem used in this article, that is a backward facing step channel flow. We also outline
the numerical methods used and present numerical results which will later be com-
pared with reduced order model predictions. In §4, we apply POD for the construction
of reduced order model. In §5, we formulate an optimal control problem and discuss
reduced order modeling approach for its solutions. We present computational results
in §6 with two different control mechanisms. Finally we conclude in §7.

1.1. Notation. We denote by $L^2(\Omega)$ the collection of square-integrable functions
defined on flow region $\Omega \subset \mathbb{R}^2$ and we denote the associated norm by $\| \cdot \|_0$. Let

$$H^1(\Omega) = \left\{ v \in L^2(\Omega) : \frac{\partial v}{\partial x_i} \in L^2(\Omega) \text{ for } i = 1, 2 \right\}$$

and the norm on it be $\| \cdot \|_1$. We denote by $L^2(0, T; H^1)$ the space of all measurable
functions $f : (0, T) \to H^1$ such that

$$\|f\|_{L^2(0,T;H^1)} = \left(\int_0^T \|f\|_1^2 dt \right)^{\frac{1}{2}} < \infty.$$

Vector-valued counterparts of these spaces are denoted by bold-face symbols, e.g.,
$\mathbf{H}^1(\Omega) = [H^1(\Omega)]^2$. The $L^2(\Omega)$ or $\mathbf{L}^2(\Omega)$ inner product is denoted by $(\cdot, \cdot)$. We denote
the inner products for $L^2(\Gamma)$ or $\mathbf{L}^2(\Gamma)$ by $(\cdot, \cdot)_\Gamma$, where Γ denotes the boundary of Ω.

2. The POD Subspace. In order to illustrate the POD subspace and its construction, we assume for the ease of exposition that we are dealing with the semi-discrete nonlinear problem

$$\frac{d\mathbf{y}}{dt} = \mathcal{E}(\mathbf{y}, t), \qquad t \in \mathbb{R} , \mathbf{y} \in \mathbf{X},$$

where $\mathbf{X}$ is a finite dimensional space. If finite element method were used to obtain the above semi-discrete problem, $\mathbf{X}$ would be a piecewise polynomial space. However, the choice for the POD subspace is different.

2.1. The Proper Orthogonal Decomposition. The underlying problem is to identify a structure in a random vector field. Given an ensemble of random vector fields $\mathbf{U}^{(i)}$, we seek to find a function $\mathbf{\Phi}$ which has a structure typical of the members of the ensemble. One way to resolve the problem is to project the ensemble on $\mathbf{\Phi}$, i.e., $(\mathbf{U}^{(i)}, \mathbf{\Phi})$, to find $\mathbf{\Phi}$ which is as nearly parallel as possible. Thus we want to maximize $(\mathbf{U}^{(i)}, \mathbf{\Phi})$ while removing the amplitude by normalizing it. It is now natural to look at a space of functions $\mathbf{\Phi}$ for which the inner-product $(\mathbf{\Phi}, \mathbf{\Phi})$ exists, i.e. $\mathbf{\Phi}$ must be $L^2(\Omega)$. In order to include the statistics, we must maximize the expression

$$(\mathbf{\Phi}, \mathbf{U}^{(i)})/(\mathbf{\Phi}, \mathbf{\Phi})^{\frac{1}{2}}$$

in some average sense. Furthermore, since we are only interested in magnitude and not the sign, we consider mean of the square of the expression. Following [23], we consider ensemble which are "snapshots", that is the ensemble set

$$\mathcal{S} = \{\mathbf{U}^{(i)} : 1 \leq i \leq N \}$$

are solutions at N different time steps t_i and seek a function $\mathbf{\Phi} \in \mathbf{L}^2(\Omega)$ that gives the best representation of $\mathcal{S}$ in the sense that it maximizes

$$\frac{1}{N} \sum_{i=1}^{N} |(\mathbf{U}^{(i)}, \mathbf{\Psi})|^2/(\mathbf{\Psi}, \mathbf{\Psi}). \tag{2.1}$$

In other words one seeks a function which has the largest mean square projection on the set $\mathcal{S}$. It was shown in [23] that when the number of degrees of freedom required to describe $\mathbf{U}^{(i)}$ is larger than the number of snapshots N, it is efficient to express the basis function as a linear combination of the snapshots. Thus we assume $\mathbf{\Phi}$ has a special form in terms of the original data as

$$\mathbf{\Phi} = \sum_{i=1}^{N} w_i \mathbf{U}^{(i)}, \tag{2.2}$$

where a_i is to determined such that $\mathbf{\Phi}$ maximizes (2.1). The maximization problem (2.1) can be cast in an equivalent eigenvalue problem. To see this define,

$$\mathbf{K}\mathbf{\Phi} = \frac{1}{N} \sum_{i=1}^{N} \int_{\Omega} \mathbf{U}^{(i)}(\mathbf{x})\mathbf{U}^{(i)}(\mathbf{x}')\mathbf{\Phi}(\mathbf{x}')d\mathbf{x}' \tag{2.3}$$

then

$$(\mathbf{K}\mathbf{\Phi}, \mathbf{\Phi}) = \frac{1}{N} \sum_{i=1}^{N} \int_{\Omega}\int_{\Omega} \mathbf{U}^{(i)}(\mathbf{x})\mathbf{\Phi}(\mathbf{x})\mathbf{U}^{(i)}(\mathbf{x}')\mathbf{\Phi}(\mathbf{x}')d\mathbf{x}d\mathbf{x}'$$

$$= \frac{1}{N} \sum_{i=1}^{N} |(\mathbf{U}^{(i)}, \mathbf{\Phi})|^2.$$

Moreover, we have

$$\frac{(\mathbf{K\Phi},\Phi)}{(\Phi,\Phi)} = \frac{\frac{1}{N}\sum_{i=1}^{N}|(\mathbf{U}^{(i)},\Phi)|^2}{(\Phi,\Phi)} = \lambda$$

Using the calculus of variations, we can find the maximum as described below: Let ϕ^* be a function that maximizes λ. We can then write any other function as $\phi^* + \epsilon\phi'$. Then λ can be written as

$$F(\epsilon) = \frac{(\mathbf{K\Phi}^*,\Phi^*) + \epsilon(\mathbf{K\Phi}^*,\Phi') + \epsilon(\mathbf{K\Phi}',\Phi^*) + \epsilon^2(\mathbf{K\Phi}',\Phi')}{(\Phi^*,\Phi^*) + \epsilon(\Phi^*,\Phi') + \epsilon(\Phi',\Phi^*) + \epsilon^2(\Phi',\Phi')} = \lambda.$$

Clearly, maximum occurs when $\epsilon = 0$ and thus $\frac{dF(\epsilon)}{d\epsilon}|_{\epsilon=0} = 0$. This leads one to

$$(\mathbf{K\Phi}^*,\Phi') = \lambda(\Phi^*,\Phi').$$

It is now clear that maximization problem (2.1) is the same as finding the eigenvalue of the eigenvalue problem

$$\mathbf{K\Phi}^* = \lambda\Phi^*. \tag{2.4}$$

If (2.2) and (2.3) are introduced into (2.4), we have

$$\mathbf{CW} = \lambda\mathbf{W},$$

where

$$\mathbf{C}_{ij} = \frac{1}{N}\int_\Omega \mathbf{U}^{(i)}(\mathbf{x})\mathbf{U}^{(j)}(\mathbf{x})d\mathbf{x} \quad \text{and} \quad \mathbf{W} = \begin{pmatrix} w_1 \\ w_2 \\ . \\ . \\ . \\ . \\ w_N \end{pmatrix}.$$

It follows from the fact that $\mathbf{C}$ is a nonnegative Hermitian matrix that it has a complete set of orthogonal eigenvectors

$$\mathbf{W}_1 = \begin{pmatrix} w_1^1 \\ w_2^1 \\ . \\ . \\ . \\ . \\ w_N^1 \end{pmatrix}, \quad \mathbf{W}_2 = \begin{pmatrix} w_1^2 \\ w_2^2 \\ . \\ . \\ . \\ . \\ w_N^2 \end{pmatrix}, \quad .... \quad , \quad \mathbf{W}_N = \begin{pmatrix} w_1^N \\ w_2^N \\ . \\ . \\ . \\ . \\ w_N^N \end{pmatrix}$$

along with a set of eigenvalues $\lambda_1 \geq \lambda_2 \geq ...... \geq \lambda_N \geq 0$. We can now write down the solutions of (2.1):

$$\Phi_1 = \sum_{i=1}^{N} w_i^1 \mathbf{U}^{(i)}, \quad \Phi_2 = \sum_{i=1}^{N} w_i^2 \mathbf{U}^{(i)}, \quad ......, \quad \Phi_N = \sum_{i=1}^{N} w_i^N \mathbf{U}^{(i)}.$$

We also normalize these by requiring

$$(\mathbf{W}_l, \mathbf{W}_l) = \sum_{i=1}^{N} w_i^l w_i^{l*} = \frac{1}{N\lambda_l}.$$

It is now easy to check

$$(\Phi_l, \Phi_m) = \begin{cases} 1 & l = m \\ 0 & l \neq m. \end{cases}$$

This completes the construction of the orthonormal set $\{\Phi_1, \Phi_2, \ldots\ldots, \Phi_N\}$. Then the POD subspace is defined as $\mathbf{V}^{POD} = \text{span}\{\Phi_1, \Phi_2, \ldots\ldots, \Phi_N\}$.

To quantify the energy of the data set associated with the corresponding mode Φ_i, we note from (2.3) that

$$\lambda_i = \frac{1}{N} \sum_{j=1}^{N} (\Phi_i, \mathbf{U}^{(j)})^2.$$

In the next section we will show that POD subspace is optimal in the sense that the approximation of the snapshots

$$\mathbf{U}^{(l)} = \sum_{i=1}^{N_k} \alpha_i^l \Phi_i, \quad \alpha_i^l = (\Phi_i, \mathbf{U}^{(l)})$$

maximizes the captured energy

$$E = \frac{1}{N} \sum_{i=1}^{N} (\mathbf{U}^{(i)}, \mathbf{U}^{(i)})$$

$$= \sum_{i=1}^{N_k} \lambda_i \quad \text{for all } N_k < N.$$

2.2. Optimality of the basis functions. Given a signal $\mathbf{u}(\mathbf{x}, t) \in \mathbf{L}^2((0, T) \times \Omega)$ and an approximation $\mathbf{u}^N$ of $\mathbf{u}$ in terms of an arbitrary orthonormal basis $\Psi_i(\mathbf{x})$, $i = $ ∎ $1, 2, \ldots\ldots, N_k$:

$$\mathbf{u}^N(\mathbf{x}, t) = \sum_{i=1}^{N_k} \alpha_i(t) \Psi_i(\mathbf{x}).$$

If $\Psi_i(\mathbf{x})$ have been nondimensionalized, then the average kinetic energy is given by

$$\left\langle \int_\Omega \mathbf{u}^N \cdot \mathbf{u}^{N*} d\Omega \right\rangle = \left\langle \sum_{i=1}^{N_k} \alpha_i(t)\alpha_i^*(t) \right\rangle,$$

where $\langle \cdot \rangle$ denotes the time average operator. We next state a proposition regarding the optimality of POD whose proof can be found in [2].

PROPOSITION 2.1. *Let* $\{\Phi_1, \Phi_2, \ldots\ldots, \Phi_{N_k}\}$ *denote an orthonormal set of POD basis elements and* $\{\lambda_1, \ldots\ldots, \lambda_{N_k}\}$ *denote the corresponding set of eigenvalues. If*

$$\mathbf{u}^N = \sum_{i=1}^{N_k} \beta_i(t) \Phi_i(\mathbf{x})$$

denotes the approximation to $\mathbf{u}$ *with respect to the basis, then the following hold:*

$(i) \quad \left\langle \beta_i(t)\beta_j^*(t) \right\rangle = \delta_{ij}\lambda_i,$

(ii) *For every* N_k, $\quad \displaystyle\sum_{i=1}^{N_k} \left\langle \beta_i(t)\beta_i^*(t) \right\rangle = \sum_{i=1}^{N_k} \lambda_i \geq \sum_{i=1}^{N_k} \left\langle \alpha_i(t)\alpha_i^*(t) \right\rangle,$

where $\mathbf{u}^N(\mathbf{x}, t) = \sum_{i=1}^{N_k} \alpha_i(t) \mathbf{\Psi}_i(\mathbf{x})$.

In essence this proposition states that among all the linear combinations, the one corresponds to POD is the best in the sense that it will capture the most kinetic energy possible in the average sense.

2.3. Model reduction aspects. To capture the underlying dynamics of the system one needs to keep N sufficiently large. Thus using a Galerkin procedure one can obtain a high fidelity model perhaps with large N. However if the eigenvalues of the covariance matrix C decays fast, one can choose a cutoff value $M \ll N$ and carry out a Galerkin procedure with a reduced set of basis elements $\{\Phi_1, \Phi_2, \ldots\ldots, \Phi_M\}$. As noted earlier, $\sum_{i=1}^{M} \lambda_i$ represents the average kinetic energy contained in the first M modes. Therefore one can choose M such that $\sum_{i=1}^{M} \lambda_i \approx \sum_{i=1}^{N} \lambda_i$ through some experimentation. Also the ratio $\frac{\sum_{i=1}^{M} \lambda_i}{\sum_{i=1}^{N} \lambda_i}$ gives the percentage of the total kinetic energy contained in the first M POD elements. In fluid flow simulations given below the POD system was constructed for $N = 100$ and the reduced order model was constructed with $M = 10$ which captured 99.99% of the energy. This clearly demonstrates the advantage of the reduced order model over the finite element model whose dimension was 3,032.

3. Simulation of Fluid Flow in a Channel. We consider two dimensional incompressible fluid flow through a channel with a backward facing step. A schematic of the geometry is given in Figure 2. The fluid flow is governed by the Navier-Stokes equations which are given by

$$\mathbf{u}_t - \tfrac{1}{Re}\Delta\mathbf{u} + \mathbf{u}\cdot\nabla\mathbf{u} + \nabla p = 0 \quad \text{in } \Omega \times (0, T),$$
$$\nabla \cdot \mathbf{u} = 0 \quad \text{in } \Omega \times (0, T), \tag{3.1}$$

where the velocity $\mathbf{u}$, the pressure p, the time t and the spatial variable $\mathbf{x}$ are in non-dimensional form. The Reynolds' number Re is defined as $Re = \rho U_0 L/\mu$, where ρ is the density, U_0 is the nondimensional velocity. The following boundary conditions are imposed.

$$
\begin{array}{rll}
\mathbf{u} &= (8(y - 1/2)(1 - y), 0) = \mathbf{u}_{\text{in}} & \text{on} \quad \Gamma_{\text{in}} \times [0, T] \\
p\mathbf{n} - \tfrac{1}{Re}\tfrac{\partial\mathbf{u}}{\partial n} &= (0, 0) & \text{on} \quad \Gamma_{\text{out}} \times [0, T] \\
\mathbf{u} &= (0, 0) & \text{on} \quad \Gamma_t \cup \Gamma_b \cup \Gamma_s \cup \Gamma_c \times [0, T].
\end{array}
$$

The boundary condition on Γ_{out} is not "physical" but used to represent the flow in an unbounded region; see [6]. For the finite dimensional approximation and for the subsequent reduced order approximation, we need a weak form of the state equations (3.1). A weak form of the equations (3.1) has the form; see [27] for similar problems,

$$(\mathbf{u}_t + \mathbf{u}\cdot\nabla\mathbf{u}, \mathbf{v}) + \tfrac{1}{Re}(\nabla\mathbf{u}, \nabla\mathbf{v}) - (p, \nabla\cdot\mathbf{v}) = 0$$
$$(\nabla\cdot\mathbf{u}, q) = 0 \tag{3.2}$$

for all test functions $(\mathbf{v}, q) \in \mathbf{V} \times L^2(\Omega)$, where

$$\mathbf{V} = \{\mathbf{v} \in \mathbf{H}^1(\Omega) : \quad \mathbf{v}|_{\Gamma\backslash\Gamma_{\text{out}}} = 0\}.$$

The state variables $(\mathbf{u}, p)$ for the problem are taken to be

$$\mathbf{u} \in L^2(0, T; \mathbf{H}^1(\Omega)), \quad \mathbf{u}|_{\Gamma_{\text{in}}} = \mathbf{u}_{\text{in}} \text{ and } \mathbf{u}|_{\Gamma\backslash\Gamma_{\text{out}}\backslash\Gamma_{\text{in}}} = 0,$$

$$p \in \mathrm{L}^2(\Omega).$$

3.1. Finite Dimensional Approximations. To approximate the solutions, we will use standard mixed finite element method. For this, we write $\mathbf{u}$ and p as linear combination of finite number of basis functions:

$$\mathbf{u}^h = \mathbf{u}_0^h + \sum_{i=1}^{N} \mathbf{u}_i(t)\Phi_i(\mathbf{x}),$$

$$p^h = \sum_{i=1}^{M} p_i(t)\Psi(\mathbf{x})$$

with $\mathbf{u}_0^h$ be the finite element interpolant of non-zero boundary conditions imposed on $\mathbf{u}$. Then

$$\mathbf{V}^N = \mathrm{span}\{\Phi_1, \Phi_2, \ldots\ldots, \Phi_N\}$$

$$Q^M = \mathrm{span}\{\Psi_1, \Psi_2, \ldots\ldots, \Psi_M\}$$

and $\mathbf{V}^N \times Q^M \subset \mathbf{V} \times L^2$. The approximate system is determined by restricting the weak form (3.2) to $\mathbf{V}^N \times Q^M$ with basis functions Φ_i substituted for the test functions $\mathbf{v}$ and the basis functions Ψ_i substituted for the test functions q. Then the following finite dimensional system results:

$$\mathbf{M}\ddot{\mathbf{u}} + \mathbf{S}\mathbf{u} + \mathbf{N}(\mathbf{u})\mathbf{u} + \mathbf{L}^T\mathbf{p} = \mathbf{F},$$

$$\mathbf{L}\mathbf{u} = 0,$$

(3.3)

where $\mathbf{S}$ is the diffusion matrix, $\mathbf{N}$ the convection matrix, $\mathbf{L}$ the continuity matrix, $\mathbf{M}$ the mass matrix and $\dot{\mathbf{u}} = \frac{d\mathbf{u}}{dt}$. Moreover $\mathbf{u}$ and $\mathbf{p}$ are the finite dimensional velocity and pressure, respectively. We call the approximations using standard finite element basis functions such as quadratic or linear piecewise polynomials by "full order methods/discretization" and the ones using POD by "reduced order methods". For the full discretization we use continuous piecewise quadratics for the velocity $\mathbf{u}$ and continuous piecewise linear functions for the pressure p; the same triangular grid is used for both finite element spaces; This choice of spaces complies with the div-stability condition which is required for stable computation of pressure; see [5].

The nonlinear differential algebraic equations (DAE) (3.3) is discretized using backward Euler in time with the time step $\Delta t = 0.01$ and the resulting nonlinear algebraic system is solved using Newtons method along with a banded Gaussian elimination.

In Figure 2, the height of the inflow boundary is 0.5 and that of the outflow boundary is 1. The length of the narrower section of the channel is 1 and that of wider section of the channel is 7. The computational domain was divided into 682 triangles with finer mesh around the recirculation region. This resulted in a system of 3,032 ordinary differential equations that has to be solved for the unknown coefficients. We choose throughout in this simulation $V_{max} = \frac{1}{2}$ and $H = 1$ with a corresponding $Re = \frac{1}{2\nu}$, where V_{max}=maximum inlet velocity, H =channel height, ν=kinematic viscosity of the fluid.

It is well known that beyond certain Reynolds' number the flow separates and a recirculation forms near the corner region. We carried out simulations at a Reynolds' number of 1000 and the long term flow simulation is given in Figure 3. It clearly predicts the re-circulations first near the corner of the step and the second one near the wall opposite to the step.

4. POD in Flow Simulation. We follow the "snapshots" approach proposed in [23] for the derivation of POD basis functions. Let $\mathbf{u}(\mathbf{x}, t)$ be a given flow field and $\{\mathbf{u}(\mathbf{x}, t_k)\}_{i=1}^{N}$ be the corresponding flow fields at N different time steps t_k, i.e. the "snapshots". We next decompose $\mathbf{u}(\mathbf{x}, t)$ as follows

$$\mathbf{u}(\mathbf{x}, t) = \mathbf{u}_m(\mathbf{x}) + \mathbf{v}(\mathbf{x}, t),$$

where $\mathbf{u}_m(\mathbf{x}) = \frac{1}{N} \sum_{k=1}^{N} \mathbf{u}(\mathbf{x}, t_k)$. We also define a spatial correlation matrix C with

$$C_{ij} = \frac{1}{N} \int_{\Omega} \mathbf{v}^i \mathbf{v}^j \, d\Omega,$$

where $\mathbf{v}^i = \mathbf{v}(\mathbf{x}, t_i)$. Then the POD basis vectors $\mathbf{\Phi}_k$ are defined by

$$\mathbf{\Phi}_k = \sum_{i=1}^{N} w_i^k \mathbf{v}^i, \quad k = 1, ..., N,$$

where w_i^k are the components of the eigenvector $\mathbf{W}^k$ of the eigenvalue problem

$$C \mathbf{W} = \lambda \mathbf{W}.$$

The computation using POD takes the following algorithmic form:

ALGORITHM I

(I)   Solve the state equation (3.3) at N different time steps and obtain
        "snapshots" $\mathcal{S}$; See Figure 1.

(II)   Compute the covariant matrix C. The matrix elements of C are
        given by $C_{ij} = \frac{1}{N} \int_{\Omega} \mathbf{v}^i \mathbf{v}^j \, d\Omega$, for $i, j = 1, 2, ..., N$.

(III)   Solve the eigenvalue problem $C\mathbf{W} = \lambda \mathbf{W}$, where C is a nonnegative
        Hermitian matrix and has a complete set of eigenvectors
        $\mathbf{W}_1, \mathbf{W}_2, ..., \mathbf{W}_N$ with $\mathbf{W}_k^T = (w_1^k, w_2^k, ..., w_N^k)$.

(IV)   Obtain the POD basis vectors Φ_i using $\Phi_i = \sum_{k=1}^{N} w_k^i \mathbf{v}^k, \ 1 \leq i \leq N$
        and define $\mathbf{V}^{POD} = \text{span}\{\Phi_1, \Phi_2, ..., \Phi_N\}$. And set $\mathbf{v} = \sum_{i=1}^{N} \alpha_i(t) \Phi_i$.

(V)   Restrict the weak form (3.2) to $\mathbf{V}^{POD}$ and solve for $\alpha_i, \ i = 1, 2, ..., N$.

(VI)   Set $\mathbf{u}(\mathbf{x}, t) = \mathbf{u}_m(\mathbf{x}) + \sum_{i=1}^{N} \alpha(t) \Phi_i$.

For the channel flow problem we obtained snapshots $\mathbf{u}(\mathbf{x}, t_i)$ of the flow at 100 regular intervals. The correlation matrix C was formed with the aid of the finite

element routine and the eigenvalue solve was carried out using the RG subroutine in the Fortran library EISPACK. The eigenvalue spectrum from the correlation matrix C is shown in Figure 4 (left). As shown in the figure, the eigenvalues quickly decay and thus very few modes capture the essential energy in the flow.

4.1. POD Reduced Order Model. In this section, we consider the construction of POD reduced order model using a Galerkin projection of the Navier-Stokes equations onto a space spanned by the POD basis elements. The nature of the POD model is that it requires fewer basis vectors than that is used to approximate the flow field. In fact the first M ($\ll N$) modes carry most of the energy in the flow and if we choose M such that

$$\sum_{i=1}^{N} \lambda_i \approx \sum_{i=1}^{M} \lambda_i,$$

we obtain a reduced order model. We found out $10 (= M)$ POD basis vectors are sufficient to capture 99% of the energy. In order to derive the reduced order model, let us apply Algorithm I, choose M and expand the solution as

$$\mathbf{u}(\mathbf{x}, t) = \mathbf{u}_m(\mathbf{x}) + \sum_{i=1}^{M} \alpha_i(t) \mathbf{\Phi}_i(\mathbf{x}). \tag{4.1}$$

Then the Galerkin approximation of the weak form (3.2) is as follows

$$(\mathbf{u}_t + \mathbf{u} \cdot \nabla \mathbf{u}, \mathbf{\Phi}_i) - (p, \nabla \cdot \mathbf{\Phi}_i) + \tfrac{1}{Re}(\nabla \mathbf{u}, \nabla \mathbf{\Phi}_i) + (p\mathbf{n} - \tfrac{1}{Re} \tfrac{\partial \mathbf{u}}{\partial \mathbf{n}}, \mathbf{\Phi}_i)_{\Gamma_{out}} = 0, \tag{4.2}$$

for all $\mathbf{\Phi}_i \in \mathbf{V}^{POD}$. At this point it is important to note that the eigenfuntions $\mathbf{\Phi}_i$ are divergence free as flow is incompressible and satisfy zero boundary conditions on $\Gamma \setminus \Gamma_{out}$. Using these properties of $\mathbf{\Phi}_i$ and the boundary condition on Γ_{out}, we see that the pressure term and the boundary terms vanishes. Then (4.2) reduces to

$$(\mathbf{u}_t + \mathbf{u} \cdot \nabla \mathbf{u}, \mathbf{\Phi}_i) + \tfrac{1}{Re}(\nabla \mathbf{u}, \nabla \mathbf{\Phi}_i) = 0, \tag{4.3}$$

for all $\mathbf{\Phi}_i \in \mathbf{V}^{POD}$. On substitution of (4.1) into (4.3) we obtain the following nonlinear evolution equation for the coefficients $\alpha_i(t)$:

$$\begin{aligned} \dot{\boldsymbol{\alpha}} &= \mathcal{A}\boldsymbol{\alpha} + \boldsymbol{\alpha}^T \mathcal{N} \boldsymbol{\alpha} + \mathbf{e}, \\ \boldsymbol{\alpha}(0) &= \boldsymbol{\alpha}_0, \end{aligned} \tag{4.4}$$

where

$$\alpha_{0i} = (\mathbf{u}_0, \mathbf{\Phi}_i), \qquad \mathcal{A}_{ij} = -(\mathbf{\Phi}_j \cdot \nabla \mathbf{u}_m, \mathbf{\Phi}_i) - (\mathbf{u}_m \cdot \nabla \mathbf{\Phi}_j, \mathbf{\Phi}_i) - \frac{1}{Re}(\nabla \mathbf{\Phi}_j, \nabla \mathbf{\Phi}_i),$$

$$e_i = -(\mathbf{u}_m \cdot \nabla \mathbf{u}_m, \mathbf{\Phi}_i) - \frac{1}{Re}(\nabla \mathbf{u}_m, \nabla \mathbf{\Phi}_i), \qquad \mathcal{N}_{ikl} = -(\mathbf{\Phi}_k \cdot \nabla \mathbf{\Phi}_l, \mathbf{\Phi}_i).$$

The solution to the above initial value problem (4.4) was obtained using an implicit Euler method for the coefficients of the POD approximation.

4.2. Numerical Results. We selected $\{t_i\}$ at hundred regular time instances in the time interval $[0, 10]$. The eigenvalue analysis of the correlation matrix resulted in M=10 and a reduced order system of dimension 10 was constructed. The initial value problem (4.4) for the nonlinear ODE was solved using backward Euler method with the time step $\Delta t = 10^{-3}$ and the resulting nonlinear algebraic system was solved using Newton iterative method. The Figures 5–6 are the channel flow computations with "full solution" and reduced order solution at time t=10 for various stations in the channel which shows excellent qualitative agreement.

In Table I, we show that ℓ_1 norm of the difference between solutions of the POD reduced order and full order solution decays as the dimension of the POD subspace increases. The percentages of the full order model energy captured by the POD reduced order model are also given in Table I which indicates only 9 basis functions were enough to capture 99.9% of the energy of the full order model.

In order to illustrate the features of the POD reduced order model, let us next compare it with another reduced order model based on the so called *reduced basis method* (RBM); see [9]. In [9] several ways to choose reduced basis subspaces were discussed. Here we consider the so called Lagrange subspace. The basis elements in the Lagrange subspace are snapshots of the problem obtained by solving the system (3.1) using a full order method. Supposing $\{\Psi_i\}_{i=1}^{M}$ denote the snapshots, the reduced order subspace is defined as $V^{RBM} = \text{span}\{\Psi_i\}_{i=1}^{M}$. Once we have a reduced order subspace V^{RBM}, the system (3.1) is projected onto V^{RBM} to obtain a reduced order model as in §4.1.

In algorithmic form the RBM can be summarized in the following form:

ALGORITHM II

(I)   Solve the state equation (3.3) at N different time steps and obtain "snapshots" $\mathcal{S}$; See Figure 1.

(II) Set $\mathbf{V}^{RBM} = \text{span}\{\Psi_1, \Psi_2, \ldots\ldots, \Psi_M\}$. And set $\mathbf{u} = \mathbf{u}_0 + \sum_{i=1}^{M} \alpha_i(t)\Psi_i$, where $\mathbf{u}_0$ account for the nonzero boundary values.

(III) Restrict the weak form (3.2) to $\mathbf{V}^{RBM}$ and solve for α_i, $i = 1, 2, \ldots., M$.

(IV) Set $\mathbf{u}(\mathbf{x}, t) = \mathbf{u}_0(\mathbf{x}) + \sum_{i=1}^{M} \alpha_i(t)\Psi_i$.

For numerical implementation of RBM, we considered, the channel flow case described earlier and compared its performance with the full order model. To generate Lagrange basis, we obtain snapshots of the model using the full order discretization at M regular time instances between $t = 0$ and $t = 10$ non-dimensional time. In order to see whether the reduced order approximation becomes more accurate as the dimension increases we computed the ℓ_1 norm of the difference between the reduced order and full order solutions. In Table II, we present the ℓ_1 norm error using $M = 3, 6, 9$ and 12 basis functions. We also report the condition numbers of the resulting mass matrices. As seen, the condition number can increase dramatically with increasing basis elements deteriorating convergence. However, the POD reduced order model do not generate such bad condition numbers as evidenced in Table I. Moreover, the POD allows easy generation of linearly independent basis elements and more stable system matrices.

5. An Optimal Control Problem. Minimization of vorticity level in flow domain is of interest in control/delay of transition of flow past bluff bodies. Thus in this section we formulate a related optimal control problem in channel flow. Flow configuration considered is a backward facing step channel. As Reynolds' number is increased, the flow separates near the corner of the step. The objective of the optimal control is to reduce the size of the recirculation and hence of the length of re-attachment. The control action is effected either through the movement of a portion of wall Γ_c or through blowing on Γ_c. In terms of boundary condition it takes the following form along the boundary Γ_c,

$$\mathbf{u} = c(t)\mathbf{g}(\mathbf{x}) \quad \text{on } \Gamma_c \times [0, T],$$

where $c(t) : [0, T] \to \mathbb{R}$ and $\mathbf{g}(\mathbf{x})$ represent respectively the temporal dependence and spatial distribution of the fluid velocity on the boundary Γ_c. The choice of cost functional or objective functional to meet the control objective of reducing the recirculation is not trivial. Here we will consider a functional of the form

$$\mathcal{J}(\mathbf{u}) = \int_0^T \|\nabla \times \mathbf{u}\|_0^2 dt$$

which corresponds to minimization of vorticity levels in the flow. The task is to find $c(t)$ or, rather, its time derivative $U = \dot{c}(t)$ such that the cost functional

$$\mathcal{J}(\mathbf{u}, U) = \frac{1}{2} \int_0^T \left\{ \|\nabla \times \mathbf{u}\|_0^2 + \beta |U|^2 \right\} dt$$

is minimized subject to the constraints that the flow fields satisfy the Navier-Stokes equations. The appearance of the second term in the cost functional $\mathcal{J}$ is necessary since we will not impose any a priori constraints on the controls. The parameter $\beta > 0$ adjusts the relative weight of the two terms in the functional and roughly speaking, β is large for expensive controls and small for inexpensive controls.

In order to obtain "snapshots" for POD basis functions, we introduce

$$\mathbf{u}_c(x) = \mathbf{u}^{c_1}(\mathbf{x}) - \mathbf{u}^{c_0}(\mathbf{x}),$$

where $\mathbf{u}^{c_1}$ is a steady flow with $c(t) = 0.1$ on Γ_c and $\mathbf{u}^{c_0}$ is that with $c(t) = 0$ on Γ_c. Then the "snapshots" are defined as

$$\mathbf{u}(\mathbf{x}, t_k) - c(t_k)\mathbf{u}_c(\mathbf{x})$$

and the basis functions $\mathbf{\Phi}_i$ as defined in Algorithm I have zero boundary conditions on the Dirichlet boundaries. The velocity expansion is defined as

$$\mathbf{u}(\mathbf{x}, t) = \mathbf{u}_m(\mathbf{x}) + c(t)\mathbf{u}_c(\mathbf{x}) + \sum_{i=1}^M \boldsymbol{\alpha}_i(t)\mathbf{\Phi}_i(\mathbf{x}) \tag{5.1}$$

so as to automatically satisfies all the Dirichlet boundary conditions.

5.1. The Reduced Order Control Problem. Inserting the expansion (5.1) into the Galerkin projection (4.3) of the Navier-Stokes equations, we obtain

$$\dot{\boldsymbol{\alpha}} + \mathcal{A}\boldsymbol{\alpha} + \boldsymbol{\alpha}^T \mathcal{N}\boldsymbol{\alpha} + U\mathbf{a} + (\mathbf{b} + \mathcal{B}\boldsymbol{\alpha})c + c^2\mathbf{d} + \mathbf{e} = 0, \tag{5.2}$$

where

$$a_i = (\mathbf{u}_c, \boldsymbol{\Phi}_i), \qquad d_i = (\mathbf{u}_c \cdot \nabla \mathbf{u}_c, \boldsymbol{\Phi}_i),$$

$$b_i = (\mathbf{u}_m \cdot \nabla \mathbf{u}_c, \boldsymbol{\Phi}_i) + (\mathbf{u}_c \cdot \nabla \mathbf{u}_m, \boldsymbol{\Phi}_i) + \frac{1}{Re}(\nabla \mathbf{u}_c, \nabla \boldsymbol{\Phi}_i),$$

$$B_{ij} = (\boldsymbol{\Phi}_j \cdot \nabla \mathbf{u}_c, \boldsymbol{\Phi}_i) + (\mathbf{u}_c \cdot \nabla \boldsymbol{\Phi}_j, \boldsymbol{\Phi}_i)$$

and $\mathcal{A}$, $\mathcal{N}$ and $\mathbf{e}$ are as defined in §4. Setting

$$\mathbf{X} = \begin{pmatrix} \boldsymbol{\alpha} \\ c \end{pmatrix}, \qquad \mathbf{A} = \begin{pmatrix} \mathcal{A} & 0 \\ 0 & 1 \end{pmatrix},$$

$$\mathbf{N(X)} = \begin{pmatrix} \boldsymbol{\alpha}^T \mathcal{N} \boldsymbol{\alpha} + (\mathbf{b} + \mathcal{B}\boldsymbol{\alpha})c + c^2 \mathbf{d} + \mathbf{e} \\ -c \end{pmatrix}, \qquad \mathbf{B} = \begin{pmatrix} \mathbf{a} \\ 1 \end{pmatrix},$$

we obtain the reduced order control problem:

$$\text{Minimize} \quad \mathcal{J}(\mathbf{X}, U) = \int_0^T \left\{ L(\mathbf{X}) + \frac{\beta}{2} U^2 \right\} dt \qquad (5.3)$$

subject to

$$\dot{\mathbf{X}} = F(\mathbf{X}) + \mathbf{B}U,$$
$$\mathbf{X}(0) = \mathbf{X}_0, \qquad\qquad (5.4)$$

where

$$L(\mathbf{X}) = \frac{1}{2}\mathbf{X}^T Q\mathbf{X} + \mathbf{X} \cdot \mathbf{f}_1 + f_2, \qquad \text{and} \qquad F(\mathbf{X}) = -\mathbf{A}\mathbf{X} - \mathbf{N(X)}.$$

At this point one can employ a variety of numerical methods designed for finite dimensional nonlinear optimal control problems such as multiple shooting methods. Our method here is based on Newtons method for the necessary condition of optimality or the so called optimality system albeit for the discrete version of it.

We further remark here that finite dimensional control systems like the one given above can also be obtained using, for example, finite element method as in §3. However, their size is too large for practical control systems whereas POD based reduced order control systems are low order and maintain high fidelity. This makes our approach extremely attractive for optimal control problems governed by partial differential equations.

5.2. Approximation of the Reduced Order Control Problem. We consider the second order discrete time approximation of (5.3)–(5.4) obtained by using the Crank-Nicholson for time discretization of (5.4) and the trapezoidal rule for the discretization of the integral in the cost functional (5.3). We obtain

$$\text{Minimize} \quad \mathcal{J}^K = \sum_{k=1}^K \left\{ \frac{1}{2} \left(L(\mathbf{X}^{k-1}) + L(\mathbf{X}^k) \right) + \frac{\beta}{2}|U^k|^2 \right\} \Delta t \qquad (5.5)$$

subject to

$$\frac{\mathbf{X}^k - \mathbf{X}^{k-1}}{\Delta t} = \frac{1}{2}\left(F(\mathbf{X}^k) + F(\mathbf{X}^{k-1})\right) + \mathbf{B}U^k, \quad 1 \leq k \leq K \tag{5.6}$$

where $K\,\Delta t = T$. Note that if $\omega \Delta t < 1$ then the mapping $\Phi(\mathbf{X}) = \mathbf{X} - \Delta t\, F(\mathbf{X})$ is dissipative, that is

$$\left(F(\mathbf{X}_1) - F(\mathbf{X}_2), \mathbf{X}_1 - \mathbf{X}_2\right) \geq (1 - \omega \Delta t)\,|\mathbf{X}_1 - \mathbf{X}_2|^2.$$

Thus for $U = \{U^k\}_{k=1}^K$, there exists a unique $\mathbf{X} = \{\mathbf{X}^k\}_{k=1}^K$ satisfying the constraint (5.6) and depending continuously on U. Moreover if $\omega \Delta t < 1$ then there exists an optimal pair $(\mathbf{X}^k, U^k)$ to problem (5.5)–(5.6).

The necessary optimality condition, see Appendix A, for (5.5)–(5.6) is given by

$$\begin{cases} \dfrac{\mathbf{X}^k - \mathbf{X}^{k-1}}{\Delta t} = \dfrac{1}{2}\left(F(\mathbf{X}^k) + F(\mathbf{X}^{k-1})\right) - \dfrac{1}{\beta}\,\mathbf{B}\mathbf{B}^T\boldsymbol{\zeta}^k \\[2mm] -\dfrac{\boldsymbol{\zeta}^{k+1} - \boldsymbol{\zeta}^k}{\Delta t} = \dfrac{1}{2}F_{\mathbf{X}}(\mathbf{X}^k)^T\left(\boldsymbol{\zeta}^k + \boldsymbol{\zeta}^{k+1}\right) + L_{\mathbf{X}}(\mathbf{X}^k) \end{cases} \tag{5.7}$$

for $1 \leq k \leq K$, with $\mathbf{X}^0 = \mathbf{X}_0$ and $\boldsymbol{\zeta}^{K+1} = 0$, and the optimal control U^k to (5.5)–(5.6) is given by

$$U^k = -\frac{1}{\beta}\,\mathbf{B}^T\boldsymbol{\zeta}^k, \quad 1 \leq k \leq K. \tag{5.8}$$

Assume that $\{U^m\}_{m=1}^\infty$ is a sequence of solutions to (5.5)–(5.6) with associated state and adjoint states $\{(\mathbf{X}^m, \boldsymbol{\zeta}^m)\}_{m=1}^\infty$ such that (5.7) holds. Let $\tilde{U}^m$ denote the step function defined by $\tilde{U}^m(t) = U^k$ on (t_{k-1}, t_k), $1 \leq k \leq K$ and $\tilde{\mathbf{X}}^m$ and $\tilde{\boldsymbol{\zeta}}^m$ be the piecewise linear functions defined by

$$\tilde{\mathbf{X}}^m(t) = \mathbf{X}^{k-1} + \frac{\mathbf{X}^k - \mathbf{X}^{k-1}}{\Delta t}(t - t_{k-1}) \quad \text{and} \quad \tilde{\boldsymbol{\zeta}}^m(t) = \boldsymbol{\zeta}^k + \frac{\boldsymbol{\zeta}^{k+1} - \boldsymbol{\zeta}^k}{\Delta t}(t - t_{k-1}).$$

Then it can be proved that the sequence $(\tilde{\mathbf{X}}^m, \tilde{U}^m, \tilde{\boldsymbol{\zeta}}^m)$ has a convergent subsequence as $\Delta t \to 0$ and for every cluster point $(\mathbf{X}, U, \boldsymbol{\zeta})$, U is an optimal control of (5.3)–(5.4) and $(\mathbf{X}, U, \boldsymbol{\zeta})$ satisfies the necessary optimality condition:

$$\begin{cases} \dot{\mathbf{X}}(t) = F(\mathbf{X}(t)) - \frac{1}{\beta}\,\mathbf{B}\mathbf{B}^T\boldsymbol{\zeta}(t) \\[2mm] -\dot{\boldsymbol{\zeta}} = F_{\mathbf{X}}(\mathbf{X})^T\boldsymbol{\zeta}(t) + L_{\mathbf{X}}(\mathbf{X}) \end{cases} \tag{5.9}$$

with $\mathbf{X}(0) = \mathbf{X}_0$ and $\boldsymbol{\zeta}(T) = 0$. Furthermore, (5.7) is a sparse system of nonlinear equations for $(\mathbf{X}, \boldsymbol{\zeta})$. We solve the system (5.7) by Newton method in our calculations of the optimal control $\{U^k\}$. The Jacobian J of equation (5.7) has the sparse structure;

$$J = \begin{bmatrix} \mathbf{A} & \mathbf{S} \\ \mathbf{Q} & -\mathbf{A}^t \end{bmatrix}$$

where $\mathbf{S}$ and $\mathbf{Q}$ are block-wise diagonal and $\mathbf{A}$ is block-wise lower bi-diagonal with block size K. The diagonal block $\mathbf{A}_{k,k}$ and the off-diagonal block $\mathbf{A}_{k+1,k}$ of $\mathbf{A}$ are given by

$$\mathbf{A}_{k,k} = \frac{I}{2\Delta t} + \frac{1}{2}F_{\mathbf{X}}(\mathbf{X}^k) \quad \text{and} \quad \mathbf{A}_{k+1,k} = -\frac{I}{2\Delta t} + \frac{1}{2}F_{\mathbf{X}}(\mathbf{X}^k).$$

S has the constant diagonal block $\frac{1}{\beta}\mathbf{B}^T\mathbf{B}$ and the diagonal block $Q_{k,k}$ of **Q** is given by

$$\mathbf{Q}_{k,k} = L_{\mathbf{XX}}(\mathbf{X}^k) + \sum_{i=1}^{K} \frac{\zeta_i^k + \zeta_i^{k+1}}{2} (F_i)_{\mathbf{x},\mathbf{x}}(\mathbf{X}^k).$$

6. Numerical Results. Here we present numerical results for the POD based control and compare its performance with that of RBM. The flow configuration is chosen as the two dimensional backward facing step. The control objective is to reduce the recirculation behind the step and thus of the re-attachment length. The cost functional is taken to be the vorticity functional defined earlier. Two control mechanisms are considered. In the first example, we consider moving wall as control and in the second we consider blowing of mass through a portion of the boundary.

6.1. Example I. In this example, the control is introduced into the problem through the movement of wall on the boundary Γ_c:

$$\mathbf{u} = c(t)\boldsymbol{\tau} \quad \text{on} \quad \Gamma_c,$$

where $\boldsymbol{\tau}$ is the unit tangential vector.

6.1.1. Test I (POD). We present numerical results for POD approach in solving the optimal control problem at $Re = 200$. Recall that the control problem we consider is

$$\text{Minimize } \mathcal{J}(\mathbf{u}, U) = \frac{1}{2}\int_0^T \left\{ \|\nabla \times \mathbf{u}\|_0^2 + \beta |U|^2 \right\} dt$$

subject to

$$(\mathbf{u}_t + \mathbf{u} \cdot \nabla \mathbf{u}, \Phi_i) + \frac{1}{Re}(\nabla \mathbf{u}, \nabla \Phi_i) = 0, \quad i=1,....,M,$$

where M is the number of POD modes and

$$\mathbf{u} = \mathbf{u}_m + c(t)\mathbf{u}_c + \sum_{i=1}^{M} \alpha_i(t)\Phi_i(\mathbf{x}).$$

The initial conditions for the states and controls are $\mathbf{u}(\mathbf{x}, 0) = 0$ and $c(0) = 0$, respectively. Our choice of the portion of the boundary Γ_c, where control is applied, is the line segment between $y = 0$ and $y = 0.5$ at $x = 1$; see Figure 2. This choice here is motivated by the fact that if one wants maximum influence in the flow, then the control has to be in that vicinity. The time interval was chosen $[0, T]$ with $T = 10$ and the number of POD modes was taken as 4. In Figures 7–9 we present numerical results for the penalty parameter $\beta = \frac{1}{50}$ and the time step $\Delta t = 0.01$. The numerical solution of the optimal control problem was obtained using the Newton's method described in §5.2. The flow fields presented in Figures 7–8 are u component of the flow field **u** for the controlled and baseline cases at different stations in the channel. As one can see when control is applied the u velocity becomes positive where it is otherwise negative and helps the formation of recirculation. Significant reduction in the recirculation bubble and re-attachment length were also observed compared to the uncontrolled case. We also carried out our calculation with different initial conditions $\mathbf{X}_0$ and the results were qualitatively similar to those described above.

6.1.2. Test II (RBM). We present here numerical results for the RBM approach to the same optimal control problem as in Test I. Like in POD, the solution expansion in RBM is of the form

$$\mathbf{u} = \mathbf{u}_0 + \sum_{i=1}^{M} \alpha_i(t)\Phi_i + \sum_{i=1}^{M_0} c_i(t)\mathbf{u}_i$$

where $\mathbf{u}_0$ denotes the flow corresponding to a zero control, i.e, it satisfies $\mathbf{u}_0 = 0$ on Γ_c, and $\mathbf{u}_1, \ldots\ldots, \mathbf{u}_{M_0}$ denotes solution of (3.1) with nonzero values on the control part of the boundary Γ_c. For the numerical results presented in Figure 9, we have used basis functions based on the data shown in Table III. For the simulation of the control problem we take

$$\mathbf{u} = \mathbf{u}_0 + \sum_{i=1}^{M} \alpha_i(t)\Phi_i + c(t)\Phi_{M+1},$$

where $M = 4$ and the basis functions $\Phi_1, \Phi_2, \Phi_3, \Phi_4$ and Φ_5 are chosen as $\Phi_1 = \mathbf{u}_4 - 2\mathbf{u}_1 + \mathbf{u}_0$, $\Phi_2 = \mathbf{u}_3 - 3\mathbf{u}_1 + 2\mathbf{u}_0$, $\Phi_3 = \mathbf{u}_4 - 4\mathbf{u}_1 + 3\mathbf{u}_0$, $\Phi_4 = \mathbf{u}_5 - 5\mathbf{u}_1 + 4\mathbf{u}_0$ and $\Phi_5 = \mathbf{u}_0 - \mathbf{u}_1$. The time interval $[0, T]$, the time step Δt, the penalty parameter and the other date were all taken the same as in the previous test case. The numerical solution of the control problem was also computed using the same method. The control distribution presented in Figure 9 and the controlled flow fields (not presented here) all agree well with that of POD. This shows the ability of RBM to provide very good controls with very few elements. However, RBM can be sensitive in terms of condition numbers of the system matrices as one increases the number of basis functions in order to improve convergence and accuracy.

6.2. Example II. In this example, we consider a different control mechanism from the previous one. The control is effected through blowing on the lower quarter of the boundary Γ_c. Thus we consider

$$\mathbf{u} = \begin{cases} c(t)\mathbf{g}(\mathbf{x}) & \text{on} \quad 0 \le y \le \frac{1}{8} \\ 0 & \text{on} \quad \frac{1}{8} < y \le \frac{1}{2} \end{cases}$$

and $\mathbf{g}(\mathbf{x}) = (10y(\frac{1}{8} - y), 0)$. The initial conditions for the states and control were $\mathbf{u}(\mathbf{x}, 0) = 0$ and $c(0) = 0$.

6.2.1. Test I (POD). We present numerical results for POD approach in solving the optimal control problem at $Re = 500$. The control is introduced into the problem through the blowing on the lower quarter of the boundary Γ_c. The computational domain was similar to Figure 2, but the length of the narrower section of the channel is 0.5 and that of wider section of the channel is 12. The computational domain was divided into 794 triangles with finer mesh around the recirculation region. Our choice of the portion of the boundary, where control is applied, is the line segment between $y = 0$ and $y = 0.125$ at $x = 0.5$. A linear time varying profile for $c(t)$ was used to generate 100 "snapshots" for the generation of POD modes. We carried out calculations with 4, 9 and 14 modes in the time interval $[0, T]$ with $T = 10$. In Figures 10–13, we present numerical results for the penalty parameter $\beta = \frac{1}{50}$. The numerical solution of the optimal control problem was obtained using the Newton's method described in §5.2. The initial conditions for the state and adjoint state were all zero and the convergence tolerance was taken to be 10^{-7}.

The controlled flow fields with 4, 9 and 14 modes showed similar results and hence only results with 9 modes are presented. The flow fields presented in Figures 10–11 are u component of the flow field **u** at different stations in the channel for the controlled and uncontrolled cases with 9 POD modes. As indicated by the controlled flow fields, separation has been effectively eliminated by the optimal blowing control. Significant reduction in the recirculation bubble and re-attachment length were also observed compared to the uncontrolled case.

6.2.2. Test II (RBM). We present here numerical results for the RBM approach. Like in POD, the solution expansion in RBM is of the form

$$\mathbf{u} = \mathbf{u}_0 + \sum_{i=1}^{M} \alpha_i(t)\Phi_i + \sum_{i=1}^{M_0} c_i(t)\mathbf{u}_i$$

where $\mathbf{u}_0$ denotes the flow corresponding to a zero control, i.e, it satisfies $\mathbf{u}_0 = 0$ on Γ_c, and $\mathbf{u}_1, \ldots\ldots, \mathbf{u}_{M_0}$ denotes solution of (3.1) with nonzero values on the control part of the boundary Γ_c. For the numerical results presented in Figure 13, we have used basis functions based on the data shown in Table IV. For the simulation of the control problem we take

$$\mathbf{u} = \Phi_1 + \sum_{i=1}^{M} \alpha_i(t)\Phi_i + c(t)\Phi_{M+1},$$

with M=4, 9 and 14, respectively. The RBM basis function selection was similar to that of the previous example. For example, when M=4, the basis functions $\Phi_1, \Phi_2, \Phi_3, \Phi_4, \Phi_5$ and Φ_6 were chosen as $\Phi_1 = \mathbf{u}_1 - 0.1(\mathbf{u}_6 - \mathbf{u}_1)/9.9$, $\Phi_2 = \mathbf{u}_2 - 1.9(\mathbf{u}_6 - \mathbf{u}_1)/9.9 - \mathbf{u}_1$, $\Phi_3 = \mathbf{u}_3 - 3.9(\mathbf{u}_6 - \mathbf{u}_1)/9.9 - \mathbf{u}_1$, $\Phi_4 = \mathbf{u}_5 - 5.9(\mathbf{u}_6 - \mathbf{u}_1)/9.9 - \mathbf{u}_1$, $\Phi_5 = \mathbf{u}_6 - 7.9(\mathbf{u}_6 - \mathbf{u}_1)/9.9 - \mathbf{u}_1$ and $\Phi_6 = \mathbf{u}_6 - \mathbf{u}_1$. The time interval $[0, T]$, the time step Δt, the penalty parameter and the other data were all taken the same as in the previous case. The numerical solution of the control problem was also computed using the same method. The control distribution presented in Figure 13 and the controlled flow fields (not presented here) all agree well with that of POD. These results seem to re-confirm our earlier observations about RBM's performance and the effectiveness of the control mechanism.

7. Conclusion. In this article we have presented a reduced order modeling approach for optimal control of fluid flows. The reduced order models suitable for control and which captures the essential physics were developed using the POD. Our computational investigations into the use of reduced order methods for control suggest promise. Significant computational savings were evidenced in the test cases considered. In the the reduced basis method there is no systematic way to increase the level of accuracy, and ill-conditioned system matrices can make it impossible to improve the accuracy. However, the POD provides a systematic and optimal way to improve the level of accuracy while maintaining well-conditioned system matrices. As we can see, these are not provided as a generic methods rather they must be used with care. Whenever they can be effective they can provide significant performance with substantially lower on-line computational resources. We have also investigated the feasibility of two different control mechanisms. Controlled flow fields in both cases were comparable. This seems to indicate that the choice of the type of control (wall movement or blowing) should be decided based on which type is the easiest to apply in the particular application.

Appendix A. We consider the problem of minimizing $\mathcal{J}(U)$ in (5.3) subject to the ordinary differential equations and initial conditions in (5.4). The control U^* is extremal and $\mathcal{J}$ has a relative minimum, if there exists an ϵ such that for all functions satisfying $\|U - U^*\| < \epsilon$ the difference $\mathcal{J}(U) - \mathcal{J}(U^*) \geq 0$. We have the following classical theorem.

THEOREM A.1. *For U^* to be extremal, it is necessary that $\delta\mathcal{J}(U^*, \delta U^*) = 0$ for all δU, where $\delta\mathcal{J}$ is the variation in $\mathcal{J}$ with respect to the variation in δU in U.*

A proof of this theorem can be found in [13]. In order to apply this theorem, let us introduce a vector of Lagrange multipliers

$$\boldsymbol{\zeta}^T = (\boldsymbol{\zeta}_1, \ldots, \boldsymbol{\zeta}_N)$$

and form an augmented functional including the constraints

$$\widehat{\mathcal{J}} = \int_0^T \left(L(\mathbf{X}) + \frac{\beta}{2}U^2 \right) + \boldsymbol{\zeta}^T \left(\dot{\mathbf{X}} - f(\mathbf{X}) - \mathbf{B}U \right) dt. \qquad (A.1)$$

We integrate by parts and take variations in $\widehat{\mathcal{J}}$ corresponding to variations δU in U to get

$$\delta\widehat{\mathcal{J}} = [-\boldsymbol{\zeta}^T \delta\mathbf{X}]_{t=T} + \int_0^T \left[L_\mathbf{X}(\mathbf{X}) + \beta U \delta U + \dot{\boldsymbol{\zeta}}^T \delta\mathbf{X} + \boldsymbol{\zeta}^T F_\mathbf{X} \delta\mathbf{X} + \boldsymbol{\zeta}^T \mathbf{B}\delta U \right] dt, \ (A.2)$$

note that $\delta\mathbf{X}(0) = 0$ as $\mathbf{X}(0)$ is given. We may eliminate some of the terms in (A.2) by defining

$$\dot{\boldsymbol{\zeta}} = -L_\mathbf{X} - \boldsymbol{\zeta}^T F(\mathbf{X}), \quad \text{and} \quad \boldsymbol{\zeta}(0) = 0. \qquad (A.3)$$

Equation (A.3) then reduces to

$$\delta\widehat{\mathcal{J}} = \int_0^T [\beta U + \boldsymbol{\zeta}\mathbf{B}] \, \delta U \, dt$$

and now from the Theorem A.1, a necessary condition for U^* to be extremal is that

$$\beta U + \boldsymbol{\zeta}^T \mathbf{B} = 0.$$

The state equation (5.4) and the *adjoint equation* (A.3) form $2n$ differential equations with boundary conditions $\mathbf{X}(0) = \mathbf{X}_0$ and $\boldsymbol{\zeta}(T) = 0$.

We like to remark here that the Theorem A.1 provides a necessary condition for optimality. It is easy to show the fact that it is in general not a sufficient optimality condition, i.e. $(\mathbf{X}^*, U^*, \boldsymbol{\zeta}^*)$ can be an extremal element without $(\mathbf{X}^*, U^*)$ being a solution to (5.3)–(5.4).

REFERENCES

[1] N. Aubry, P. Holmes, J. L. Lumley and E. Stone, *The dynamics of coherent structures in the wall region of a turbulent boundary layer*, Journal of Fluid Mechanics, **192** (1988), pp. 115–173.

[2] G. Berkooz, P. Holmes and J. L. Lumley, *The proper orthogonal decomposition in the analysis of turbulent flows*, Annual Review of Fluid Mechanics, **25**(5) (1993), pp. 539–575.

[3] K. S. Ball, L. Sirovich and L. R. Keefe, *Dynamical eigenfunction decomposition of turbulent channel flow*, International Journal for Numerical Methods in Fluids, **12** (1991), pp. 585–604.

[4] J. A. Burns and Y.-R. Ou, *Feedback control of the driven cavity problem using LQR Designs*, Proc. 33rd IEEE Conference on Decision and Control, Florida, **33** (1994), pp. 289-294.

[5] M. D. Gunzburger, *Finite Element Methods for Viscous Incompressible Flows*, Academic Press Inc., London, 1989.

[6] J. G. Heywood, *Artificial boundaries and flux and pressure conditions for the incompressible Navier-Stokes equations*, Preprint 94-06, SFB 359, Universitat Heidelberg, 1994.

[7] L. S. Hou and S. S. Ravindran, *A penalized Neumann control approach for solving an optimal Dirichlet control problem for the Navier–Stokes equations*, SIAM Journal on Control and Optimization, **36**(5) (1997), pp. 1795–1814.

[8] ———, *Computations of boundary optimal control problems for an electrically conducting fluid*, Journal of Computational Physics, **128**(2) (1996), pp 319–330.

[9] K. Ito and S. S. Ravindran, *A reduced order method for simulation and control of fluid flows*, Journal of Computational Physics, **143** (1998), pp. 403–425.

[10] R. D. Joslin, M. D. Gunzburger, R. Nicolaides, G. Erlebacher and M. Y. Hussaini, *A Self-contained, automated methodology for optimal flow control validated for transition delay*, AIAA Journal, **35** (1997), pp. 816–824.

[11] K. Karhunen, *Zur spektral theorie stochasticher prozesse*, Ann. Acad. Sci. Fennicae, Ser. A1 Math Phys., **37** (1946).

[12] M. Kirby, J. P. Boris and L. Sirovich, *A proper orthogonal decomposition of a simulated supersonic shear layer*, International Journal for Numerical Methods in Fluids, **10** (1990), pp. 411–428.

[13] D. E. Kirk, *Optimal Control Theory*, Prentice Hall, Englewood Cliffs, NJ, 1970.

[14] M. Loeve, *Functiona aleatoire de second ordre*, Compte Rend. Acad. Sci., Paris, (1945), pp. 220.

[15] J. L. Lumley, *The structure of inhomogeneous turbulence*, in Atmospheric Turbulence and Radio Wave Propagation, A.M. Yaglom and V.I. Tatarski, eds., Nauka, Moscow, 1967, pp. 166–178.

[16] D. V. Maddalon, F. S. Collier, F. S. Montoya and C. K. Land, *Transition flight experiments on a swept wing with suction*, AIAA Paper 89-1893.

[17] V. J. Modi, F. Mokhtarian, M. Fernando and T. Yokomizo, *Moving surface boundary-layer control as applied to two-dimensional airfoils*, J. Aircraft, **28** (1991), pp. 104-112.

[18] P. Moin and R. D. Moser, *Characteristic-eddy decomposition of turbulence in a channel*, Journal of Fluid Mechanics, **200** (1989), pp. 417–509.

[19] D. S. Park, D. M. Ladd and E. W. Hendricks, *Feedback control of Kármán vortex shedding*, Symposium on Active Control of Noise and Vibration, 19–ASME Winter Annual Meeting, Anaheim, CA, 1992.

[20] M. Rajaee, S. K. F. Karlson and L. Sirovich, *Low dimensional description of free shear flow coherent structures and their dynamical behavior*, Journal of Fluid Mechanics, **258** (1994), pp. 1401–1402.

[21] K. Roussopoulos, *Feedback control of vortex shedding at low Reynolds' numbers*, J. Fluid Mech., **248** (1993), pp. 267–296.

[22] A. SEIFERT, A. DARABI AND I. WYGANSKI, *Delay of airfoil stall by periodic excitation*, Journal of Aircraft, **33**(4) 1996.

[23] L. SIROVICH, *Turbulence and the dynamics of coherent structures: Part I–III*, Quarterly of Applied Mathematics, **45**(3) (1987), pp. 561–590.

[24] L. SIROVICH, *Analysis of turbulent flows by means of the empirical eigenfunctions* Fluid Dynamics Research, **8** (1991), pp. 85–100.

[25] B. L. SMITH AND A. GLEZER, *Vectoring and small scale motions effected in free shear flows using synthetic jet actuators*, AIAA Paper 97-0213.

[26] S. S. SRITHARAN, *An optimal control problem in exterior hydrodynamics*, Proc. of the Royal Society of Edinburgh, **121**A (1992), pp. 5–32.

[27] R. TEMAM, *Navier-Stokes Equations and Nonlinear Functional Analysis*, SIAM, Philadelphia, PA, 1983.

TABLE I. ℓ_1 *norm difference between full order and POD reduced order model solutions, condition numbers of the mass matrix and percentage of full order model energy captured with* $M = 3, 6, 9, 12, 15$ *and 20 POD basis functions.*

M	3	6	9	12	15	20
ℓ_1 Error	0.0013	0.001	.000769	0.000359	0.00029	0.00017
Condition # κ	1.0	1.0	1.0	1.0	1.0	1.0
% of Energy	97.0	99.68	99.96	99.997	99.999	99.9999

TABLE II. ℓ_1 *norm difference between full order and RBM reduced order model solutions and condition numbers of the mass matrix with* $M = 3, 6, 9$ *and 12 basis functions.*

M	3	6	9	12
ℓ_1 Error	0.0327	0.0057	.0035	0.0023
Condition # κ	613.45	21840	388556	1974595

TABLE III. *Simulation data for RBM reduced order model; Example I.*

	$\mathbf{u}_0$	$\mathbf{u}_1$	$\mathbf{u}_2$	$\mathbf{u}_3$	$\mathbf{u}_4$	$\mathbf{u}_5$
Control	0	-0.1	-0.2	-0.3	-0.4	-0.5

TABLE IV. *Simulation data for RBM reduced order model with 4, 9 and 14 mode, respectively; Example II.*

	$\mathbf{u}_1$	$\mathbf{u}_2$	$\mathbf{u}_3$	$\mathbf{u}_4$	$\mathbf{u}_5$	$\mathbf{u}_6$	$\mathbf{u}_7$	$\mathbf{u}_8$	$\mathbf{u}_9$	$\mathbf{u}_{10}$	$\mathbf{u}_{11}$	$\mathbf{u}_{12}$	$\mathbf{u}_{13}$	$\mathbf{u}_{14}$	$\mathbf{u}_{15}$	$\mathbf{u}_{16}$
Control	0.1	2	4	6	8	10										
Control	0.1	1	2	3	4	5	6	7	8	9	10					
Control	0.1	1	2	3	4	5	5.5	6	6.5	7	7.5	8	8.5	9	9.5	10
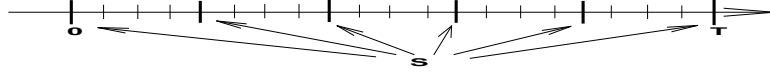
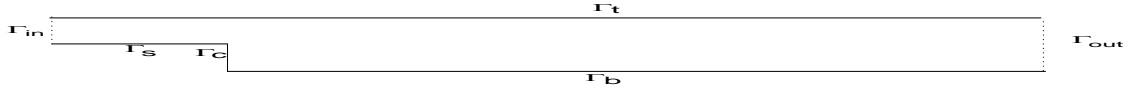FIG. 1. *Illustration of sample selection ("snapshots") for reduced order methods.*

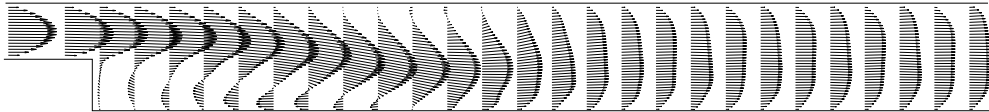FIG. 2. *Computational domain for the backward-facing-step channel problem*
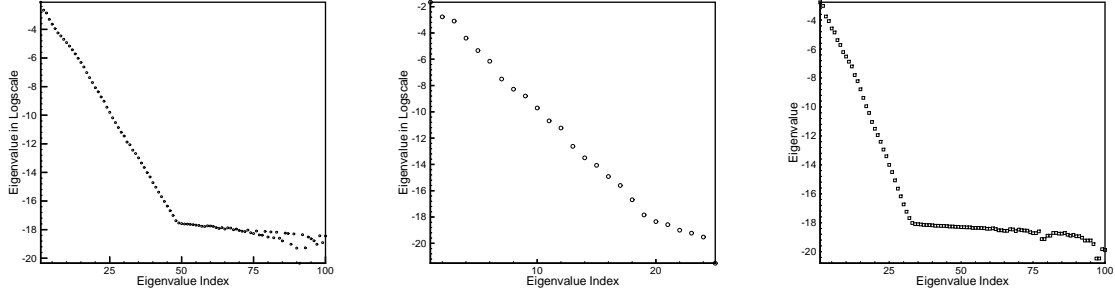

FIG. 3. *Velocity field at $t = 10$ and Re=1000.*

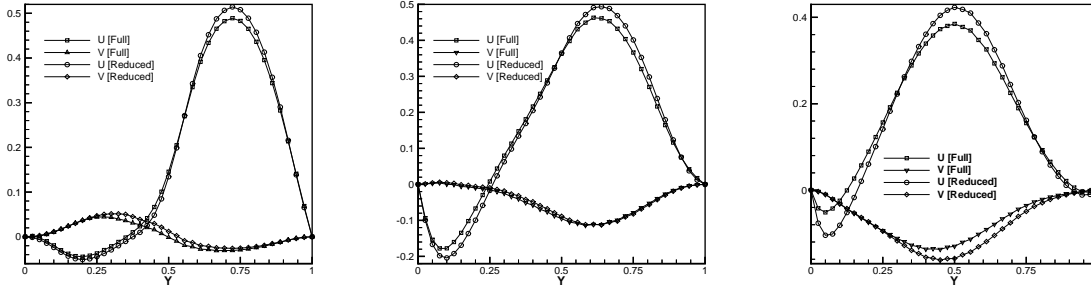FIG. 4. *Eigenvalues of the correlation matrix for the baseline and controlled cases (Test I and II), respectively*

FIG.5. *Comparison of full model versus reduced model solutions; velocity components u and v at* $x = 1.31$, $x = 1.9$ *and* $x = 2.38$
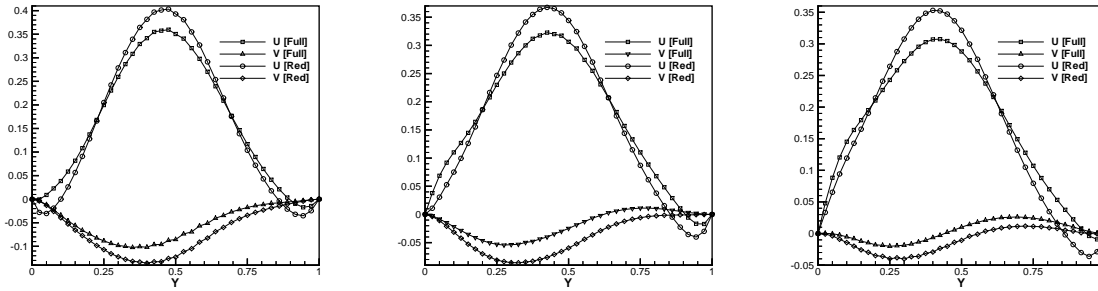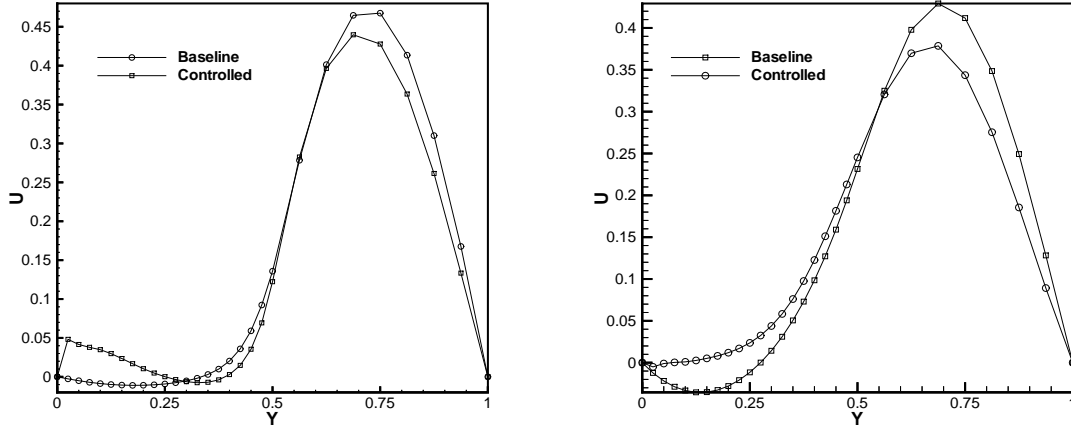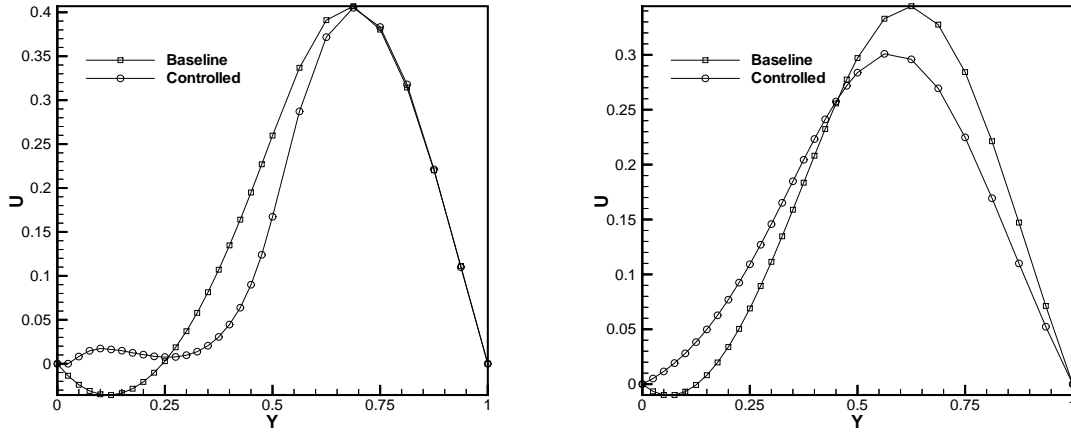

FIG. 6. *Comparison of full model versus reduced model solutions; velocity components u and v at* $x = 2.53$, $x = 2.69$ *and* $x = 2.84$
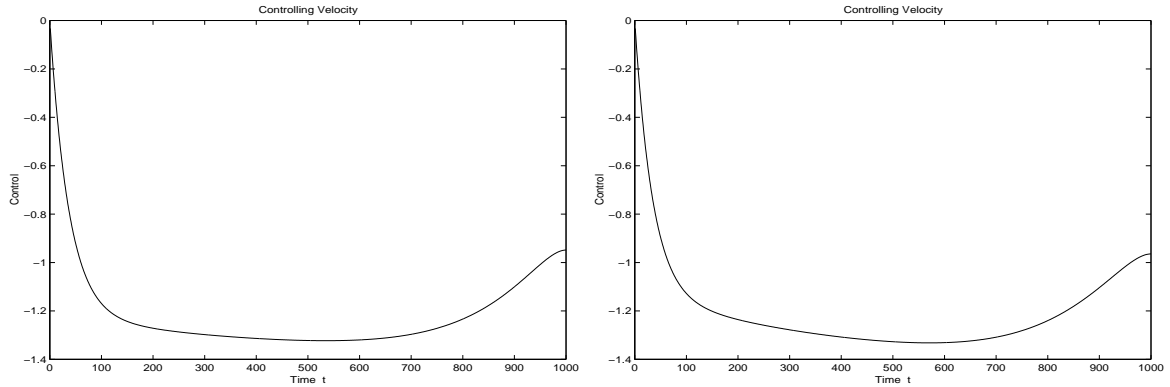
FIG . 7. *Uncontrolled vs controlled u at x = 1.2 and at x = 1.31, respectively*

FIG . 8. *Uncontrolled vs controlled u at x = 1.5 and at x = 1.9, respectively*

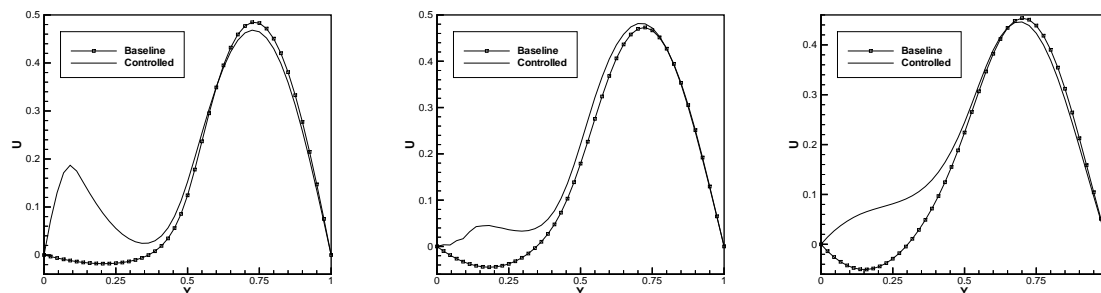FIG . 9. *Control inputs using POD (Test I) and RBM (Test II), respectively*

FIG. 10. *Uncontrolled vs controlled u at x = 0.725, x = 0.95 and at x = 1.17,*
respectively

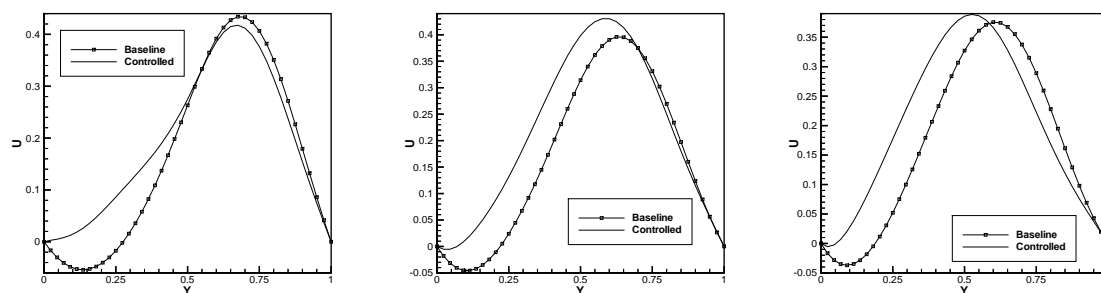FIG. 11. *Uncontrolled vs controlled u at x = 1.4, x = 1.85 and at x = 2.075,*
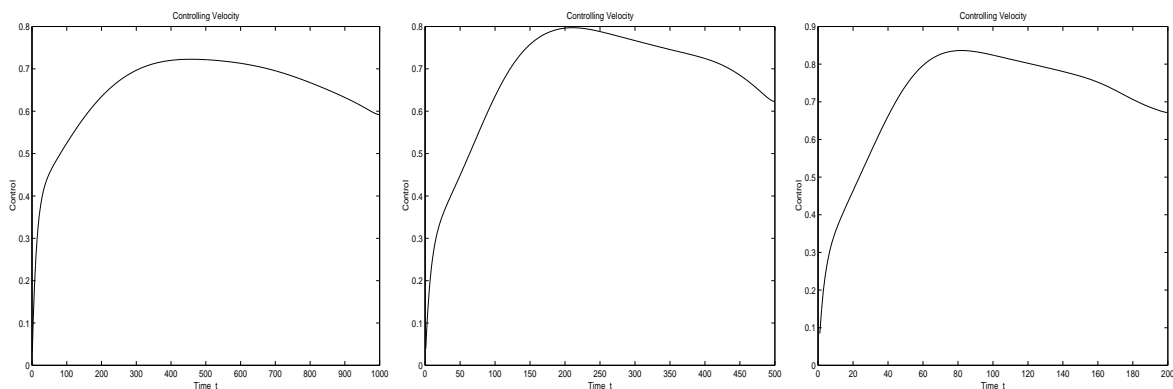*respectively*

FIG. 12. *Optimal controls using 4,9 and 14 POD modes; Test I*

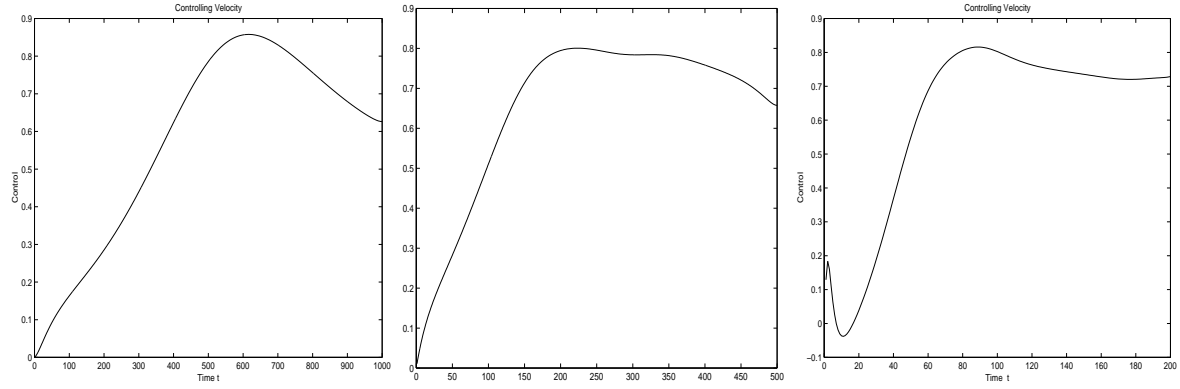FIG. 13. *Optimal controls using 4,9 and 14 RBM basis elements; Test II*

REPORT DOCUMENTATION PAGE

Public reporting burden for this collection of information is estimated to average 1 hour per response, including the time for reviewing instructions, searching existing data sources, gathering and maintaining the data needed, and completing and reviewing the collection of information. Send comments regarding this burden estimate or any other aspect of this collection of information, including suggestions for reducing this burden, to Washington Headquarters Services, Directorate for Information Operations and Reports, 1215 Jefferson Davis Highway, Suite 1204, Arlington, VA 22202-4302, and to the Office of Management and Budget, Paperwork Reduction Project (0704-0188), Washington, DC 20503.

1. AGENCY USE ONLY *(Leave blank)*	2. REPORT DATE March 1999	3. REPORT TYPE AND DATES COVERED Technical Memorandum

4. TITLE AND SUBTITLE
Proper Orthogonal Decomposition in Optimal Control of Fluids

5. FUNDING NUMBERS
WU 522-32-31-01

6. AUTHOR(S)
S. S. Ravindran

7. PERFORMING ORGANIZATION NAME(S) AND ADDRESS(ES)

Langley Research Center
Hampton, Virginia 23681-2199

8. PERFORMING ORGANIZATION REPORT NUMBER

L-17846

9. SPONSORING/MONITORING AGENCY NAME(S) AND ADDRESS(ES)

National Aeronautics and Space Administration
Washington, DC 20546-0001

10. SPONSORING/MONITORING AGENCY REPORT NUMBER

NASA/TM-1999-209113

11. SUPPLEMENTARY NOTES
Ravindran: NRC-Resident Research Associate, Langley Research Center, Hampton, VA

12a. DISTRIBUTION/AVAILABILITY STATEMENT
Unclassified-Unlimited
Subject Category 34   Distribution: Standard
Availability: NASA CASI (301) 621-0390

12b. DISTRIBUTION CODE

13. ABSTRACT *(Maximum 200 words)*

In this article, we present a reduced order modeling approach suitable for active control of fluid dynamical systems based on proper orthogonal decomposition (POD). The rationale behind the reduced order modeling is that numerical simulation of Navier-Stokes equations is still too costly for the purpose of optimization and control of unsteady flows. We examine the possibility of obtaining reduced order models that reduce computational complexity associated with the Navier-Stokes equations while capturing the essential dynamics by using the POD. The POD allows extraction of certain optimal set of basis functions, perhaps few, from a computational or experimental data-base through an eigenvalue analysis. The solution is then obtained as a linear combination of these optimal set of basis functions by means of Galerkin projection. This makes it attractive for optimal control and estimation of systems governed by partial differential equations. We here use it in active control of fluid flows governed by the Navier-Stokes equations. We show that the resulting reduced order model can be very efficient for the computations of optimization and control problems in unsteady flows. Finally, implementational issues and numerical experiments are presented for simulations and optimal control of fluid flow through channels.

14. SUBJECT TERMS
POD; reduced order model; flow control; optimal control; Galerkin methods

15. NUMBER OF PAGES
30

16. PRICE CODE
A03

17. SECURITY CLASSIFICATION OF REPORT Unclassified	18. SECURITY CLASSIFICATION OF THIS PAGE Unclassified	19. SECURITY CLASSIFICATION OF ABSTRACT Unclassified	20. LIMITATION OF ABSTRACT UL

NSN 7540-01-280-5500

Standard Form 298 (Rev. 2-89)
Prescribed by ANSI Std. Z-39-18
298-102